AIP | Advances

Studies on linear, nonlinear optical and excited state dynamics of silicon nanoparticles prepared by picosecond laser ablation

Syed Hamad, G. Krishna Podagatlapalli, R. Mounika, S. V. S. Nageswara Rao, A. P. Pathak, and S. Venugopal Rao

Citation: AIP Advances **5**, 127127 (2015); doi: 10.1063/1.4939017
View online: http://dx.doi.org/10.1063/1.4939017
View Table of Contents: http://scitation.aip.org/content/aip/journal/adva/5/12?ver=pdfcov
Published by the AIP Publishing

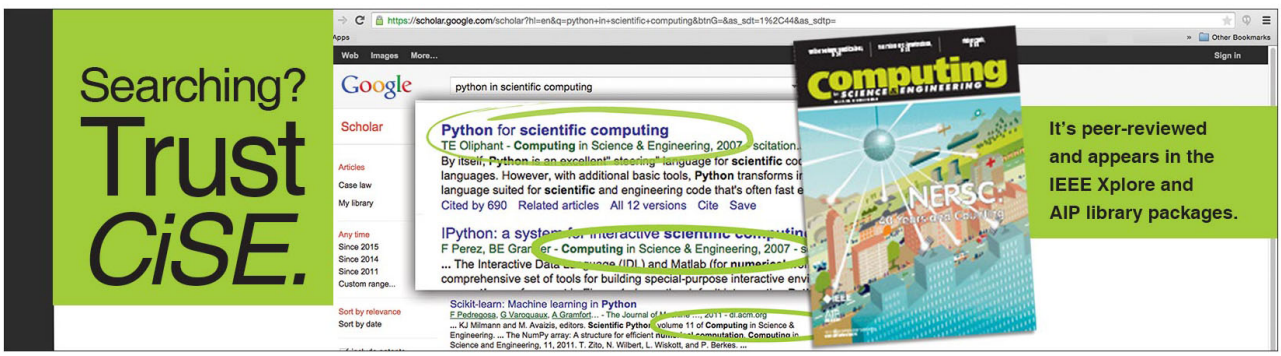

AIP ADVANCES **5**, 127127 (2015)

Studies on linear, nonlinear optical and excited state dynamics of silicon nanoparticles prepared by picosecond laser ablation

Syed Hamad,[1] G. Krishna Podagatlapalli,[2] R. Mounika,[2]
S. V. S. Nageswara Rao,[1] A. P. Pathak,[1] and S. Venugopal Rao[2,a]
[1]*School of Physics, University of Hyderabad, Hyderabad 500046, Telangana, India*
[2]*Advanced Center of Research in High Energy Materials (ACRHEM), University of Hyderabad, Hyderabad 500046, Telangana, India*

(Received 27 July 2015; accepted 7 December 2015; published online 21 December 2015)

We report results from our studies on the fabrication and characterization of silicon (Si) nanoparticles (NPs) and nanostructures (NSs) achieved through the ablation of Si target in four different liquids using ~2 picosecond (ps) pulses. The consequence of using different liquid media on the ablation of Si target was investigated by studying the surface morphology along with material composition of Si based NPs. The recorded mean sizes of these NPs were ~9.5 nm, ~37 nm, ~45 nm and ~42 nm obtained in acetone, water, dichloromethane (DCM) and chloroform, respectively. The generated NPs were characterized by selected area electron diffraction (SAED), high resolution transmission microscopy (HRTEM), Raman spectroscopic techniques and Photoluminescence (PL) studies. SAED, HRTEM and Raman spectroscopy data confirmed that the material composition was Si NPs in acetone, Si/SiO_2 NPs in water, Si-C NPs in DCM and Si-C NPs in chloroform and all of them were confirmed to be polycrystalline in nature. Surface morphological information of the fabricated Si substrates was obtained using the field emission scanning electron microscopic (FESEM) technique. FESEM data revealed the formation of laser induced periodic surface structures (LIPSS) for the case of ablation in acetone and water while random NSs were observed for the case of ablation in DCM and chloroform. Femtosecond (fs) nonlinear optical properties and excited state dynamics of these colloidal Si NPs were investigated using the Z-scan and pump-probe techniques with ~150 fs (100 MHz) and ~70 fs (1 kHz) laser pulses, respectively. The fs pump-probe data obtained at 600 nm consisted of single and double exponential decays which were tentatively assigned to electron-electron collisional relaxation (<1 ps) and non-radiative transitions (>1 ps). Large third order optical nonlinearities (~10^{-14} e.s.u.) for these colloids have been estimated from Z-scan data at an excitation wavelength of 680 nm suggesting that the colloidal Si NPs find potential applications in photonic devices. [http://dx.doi.org/10.1063/1.4939017]

I. INTRODUCTION

The promise of silicon (Si) based fluorescent labels for bioimaging[1,2] has prompted enormous attention towards Si nanoparticles (NPs) due to their direct band gap transitions, which is a consequence of quantum confinement. In recent years, Si NPs and nanostructures (NSs) have been recognized to be promising materials due their remarkable optical properties leading to several potential applications such as in optoelectronic devices,[3] light emitting devices[4] and biomedicine.[5] Over the last two decades, directed research towards synthesis/fabrication of Si NPs have demonstrated that the optical and electronic properties of Si NPs are purely size dependent. Si NPs with size <10 nm

[a]Corresponding Author: soma_venu@yahoo.com OR soma_venu@uohyd.ac.in

demonstrated photoluminescence (PL) in the 400-700 nm spectral range.[6,7] Moreover, the surface passivation of NPs depend on organic molecules present in the liquid medium. The interaction of these Si NPs with organic components in liquid media could form an organic layer on the surface of NP that make changes in the electronic energy level system resulting in the observation of red/blue shift in the PL spectra.[8] Furthermore, surface and size of the NPs play crucial roles in deciding the features of PL in the visible spectral range[9–14] and third-order optical nonlinearities. Such type of NPs are preferred for solution- processed photo detectors[15] and biomedical applications.[16,17] The wet chemistry based methods[18–21] are easy and faster for synthesizing colloidal nanoparticle solutions of metals and silica. However, these methods were not successful in the case of Si since high temperature and highly reducing agents are required to prepare Si NPs. Ultrafast laser ablation in liquid media (ULAL) has emerged to be one of the fast and effortless methods in recent times for the preparation of nanomaterials (NMs) compared to other techniques since it does not require multistep chemical synthetic procedures, long reaction times, and temperature treatments.[22–30] Furthermore, ULAL, being a green technique, promises production of stable NPs without the use of any harmful chemical precursors and are deemed safe since the fabricated NPs will remain in colloidal rather than powder form. The other noteworthy advantage of ULAL technique, in comparison with other chemical/physical approaches, is that both NPs and NSs can be fabricated in a single experiment. Over the last few years ULAL has been exploited to demonstrate (a) superior size and structural characteristics (b) enhanced crystalline phase of the generated NPs (c) significantly reduced propensity towards agglomeration in the generation of various NPs.[28] Recently, our group reported the fabrication of Si NPs under the influence of pulse energies by fs ablation of silicon in liquid media with tunable PL properties.[31] We have also achieved sub-wavelength sized NSs on the Si surface in the same experiment (single exposure).[31] In these studies[31] we had used femtosecond (fs) pulses for ablating the Boron doped p-type Si (100) target with very low resistivity (<0.005 Ω-cm) and investigated the effect of varying input energies (10-500 μJ). In the present case, however, we have performed the ablation studies with ~2 ps pulses and different liquid media (acetone, chloroform, DCM, and water) for a fixed input energy of ~150 μJ. Ps ablation has an added advantage that one can achieve faster ablation rates and thereby resulting in higher yields (grams/hour) of the NPs.[32] Further, ablation with ps and fs pulses vary slightly in their dynamics and, therefore, NPs with different sizes are expected in each case. Table I summarizes some of the recently reported Si NPs obtained with ps and fs ablation techniques in different liquids and obviously the properties of obtained NPs were different in each case. NPs with different sizes exhibit diverse optical properties thereby providing the ability to tune them and achieve desired outcome (e.g. PL peak wavelength). Additionally, laser induced surface structures on the surfaces of metal targets have also been generated along with the NPs in our experiments.[33–41] Several research groups have also investigated the formation of laser induced periodic surface structures (LIPSS) in semiconductors especially in silicon.[42–45] In the ultrashort pulse regime, the production of LIPSS depends on the laser fluence which could be approximately equal to the threshold fluence of the material.

There are sporadic reports on the nonlinear optical (NLO) studies of Si NPs produced by laser ablation in liquid media.[46] Particularly, Si NPs have been investigated extensively for third order NLO properties since they possess large third order and fifth order nonlinearities compared to other NCs leading to optical switching, optical signal processing and optical limiting applications. Different research groups have demonstrated the existence of large nonlinearities in Si NPs synthesized by other physical and chemical methods.[47–50] Along with NLO properties, excited state relaxation dynamics of electrons have attracted attention in coinage metals due to their real time applications in the fields of optical data storage systems and ultrafast communication systems.[51–53] These dynamical properties can be tuned principally by optimizing the size, shape, solvent[54–56] and synthesis technique of NPs. The transient signature of metal NPs can be obtained by the excitation of surface Plasmons and the coherent spike in this transient signature disappears when the collective oscillations of excitons drop their phase. Subsequently, the distribution of energy takes place in the electron system and later transferred to the lattice system of NP owing to the thermalization process. These thermalization processes can be monitored by employing time resolved pump-probe techniques[57–59] In this technique, ultrafast pulses cause the excitation of SPR band

TABLE I. Summary of Si NPs obtained using ps and fs ablation techniques in different solvents and reported by various groups.

Sample	Laser Parameters	Si NPs Properties	Ref.
(001) Silicon with resistivity >8,000 Ohms cm	387 nm, 180 fs, 1 kHz, pulse energy 3.5 J (fluence 0.8 J/cm^2) 70 minutes ablation	~20 nm	22
Silicon micro particles (from Si wafer) 0.08 to 1 g L^{-1} concentration	1025 nm, 480 fs, 1 kHz initial diameter of 2.3 mm focused by a 75 mm lens exposed for 45 minutes	2–3 nm (<2.5 nm distribution) for low concentrations 20–25 nm (<10 nm size distribution) for high concentrations	23
Si target (99.999%) In quartz cuvette	110 fs centered at 800 nm, 1 kHz, 0.15-0.4 mJ,	65 nm (high energy regime) 5.5 nm (low energy regime)	28
99.999% Si cylinder diameter of 6 mm and thickness of 10 mm	800 nm, energy of 1 mJ/pulse at a repetition rate of 1 kHz, 100 fs spot size of 500 μm Pulse energies from 0.05 to 0.5 mJ	0.16 J energy - 2.5 nm (±1.2) 0.27 J energy - 3.5 nm (±1.7) 0.40 J energy - 60 nm (±0.6)	29
Si cylinder target diameter of 6 mm and a thickness of 10 mm	355 nm, 60 ps, 20 Hz, 1 mJ energy used; 60 minutes of ablation	5 minutes ablation – 10 nm size 60 minutes ablation – 2 nm	77
Si plate in an aqueous solution of protein A	800 nm, pulse duration of 100 fs repetition rate of 1 kHz 10 cm focal length 0.12 mJ pulse energy for 15 min	Bio-conjugated Si-NPs mean size of 8 nm Si-NPs in deionized water 15 nm	86
<111>plane Silicon wafer in ethanol	800 nm, 50 fs, 1 kHz, two delayed fs pulses (0-4 ps)	46 nm (0 fs delay), 5.9 nm (100 fs delay), 15.2 nm (200 fs delay), 8.8 nm (1 ps delay)	89
Crystalline Silicon (KEF, 111-orientation, n-type) 400 μm thick; target area was about 1 cm^2.	1028 nm, 10 nm spectra width, 120 μJ max. energy, 5 kHz repetition rate, focused using 10× microscope objective; distilled water used	Mean diameter of 4-6 nm 1-18 nm sized particles	90

which can provide both radiative transitions (electron-electron relaxation) and thermal relaxations such as electron-phonon relaxation and phonon-phonon relaxation. The thermal process depends on the fluence of the pump pulse. Ultrafast time resolved spectroscopy was exploited to investigate electron dynamics such as electron–electron relaxation and electron–phonon relaxations of metallic films with thickness of 10-100 nm.[60–64] Specifically, Ahmadi et al.[65,66] demonstrated both electron-phonon relaxations and phonon-phonon relaxation for Au NPs (30 nm) at excitation wavelengths of 380 nm and 600 nm. Ag NPs (10 nm) also exhibited two life times of ~2 ps and ~40 ps when NPs were probed within the range of 660-790 nm by fs pump-probe spectroscopy.[67] Similar lifetime was observed in the case of Ag NPs with size in the range of 10-50 nm by other groups.[68] Tokizaki et al.[69] reported that Cu NPs in glass template also showed comparable life time of ~0.4 ps which was attributed to the electron-electron relaxation. In contrast, semiconductor NPs demonstrated only two kinds of relaxation dynamics which are electron-phonon decay (> 2 ps) and phonon-phonon decay (> 10 ps).[70,71] Especially, colloidal Si NPs with different sizes depicted two life times of 1-2 ps and 10-15 ps and the results confirmed that size dependent life times were also possible.[72] Our research group[73–75] has recently reported the fs excited state dynamics of organic moieties in solution form using degenerate pump-probe technique at 600 nm. In the present communication we report the fabrication and characterization of silicon (Si) nanoparticles (NPs) and nanostructures (NSs) achieved through the ablation of Si target in four different liquids using ~2 ps pulses. The influence of liquid media on the ablation of Si target was investigated by studying the surface morphology along with material composition of Si based NPs. The generated

NPs were characterized by selected area electron diffraction (SAED), high resolution transmission microscopy (HRTEM), Raman spectroscopic techniques and Photoluminescence (PL) studies. Femtosecond (fs) nonlinear optical and excited state dynamics of these colloidal Si NPs were investigated using the Z-scan and pump-probe techniques with ~150 fs (680 nm, 100 MHz) and ~70 fs (600 nm, 1 kHz) laser pulses, respectively.

II. EXPERIMENTAL DETAILS

The ablation studies were carried out by a 1 kHz chirped pulse amplified Ti: sapphire laser system (LEGEND, Coherent) delivering nearly bandwidth limited laser pulses (~2 ps) at 800 nm. The amplifier was seeded with large bandwidth (~15 fs) pulses from an oscillator (MICRA, Coherent). The diameter of input laser beam was ~8 mm and was focused with a convex lens (focal length 25 cm) on the surface of Si substrate placed in different solvents such as acetone, water, DCM and chloroform. Typical input pulse energy utilized was ~150 μJ. The pulse energy was controlled by a combination of Brewster angle polarizer and a half wave plate. The target was placed normal to the laser beam on a Nano-Direct three dimensional motorized stage with motion controller (~25 nm resolution) which was interfaced to a computer. The beam diameter, estimated experimentally at the focus on the sample surface in the liquid media of 5 mm thickness, was found to be ~90 μm. The volume of the liquid used was ~10 ml. Duration of each scan was ~30 minutes and line to line spacing was ~60 μm. To avoid any ambiguity in identification, the generated colloidal Si NPs were labeled as SiNP1, SiNP2, SiNP3 and SiNP4 for samples prepared in liquids of Acetone, Water, DCM, and Chloroform, respectively. Surface morphology and crystallinity of Si NPs were confirmed by utilizing the TEM, HRTEM and SAED techniques. These measurements were performed with SEI cecnai G2 S-Twin **200 kV** instrument by placing a drop of metallic colloids on carbon coated copper grids and incubated for 24 hrs to dry the sample at room temperature. The Raman and PL spectra of all colloidal Si NPs were recorded by placing NPs on a glass cover slip and allowing them to dry for ~1 hour. The spectra were recorded using a WITec Alpha 300 spectrometer with excitation wavelengths of 532 nm (CW) and 355 nm (CW). The sample on the cover slip was easily recognized through the in-built optical microscope (with an objective lens of 40X) and the spectrum was collected by the in-built spectrometer in the WITec instrument simultaneously. To avoid the heating effect through the accumulation, low power (5 mW) was used for both the studies. UV-Visible extinction spectra (Jasco V-670) were recorded for colloidal Si NPs to find out characteristic absorption peak position. Similarly, surface morphologies of the laser ablated areas of the Si substrates were carried out through a scanning electron microscopy (SEM) [Ultra 55 from Carl ZEISS with 5 kV accelerating voltage] instrument.

A Ti:sapphire laser oscillator (Chameleon, Coherent) was used to investigate NLO properties of Si NPs in solution form at 680 nm wavelength which was pumped with a Nd:YVO_4 laser operating at 527 nm in Verdi, generating pulses of 80 MHz repetition rate and ~140 fs pulse duration. This source was tunable from 680 nm to 1080 nm with 800 nm being the central wavelength. The laser beam passes through the plano-convex lens of focal length 10 cm and the sample was moved along the beam propagation path via the focal point and recorded scanned transmittance data manually at every Z position using the detector (Thermal Sensor, Field-Max). The input intensity was cut down by using neutral density filters. The estimated beam waist diameter was to be ~30 μm and corresponding Rayleigh range (Z_r) of ~2 mm which guarantees the validity of thin sample approximation since the sample length was $<<Z_r$. Typically, the peak intensities used for the open and closed apertures were ~0.38 GW/cm^2 and ~0.1 GW/cm^2, respectively.

The degenerate pump-probe experiments were carried out using ~70 fs pulses from an optical parametric amplifier (OPA- TOPAS-C, Light Conversion, Coherent) delivered at 1 kHz repetition rate with wavelength tunable in the 200–2000 nm spectral region. The average power of the pulses was ~150 mW. The OPA was pumped by the Ti: sapphire amplifier delivering ~40 fs pulses with central wavelength of 800 nm and ~2.5 W average power. The pump-probe studies were performed at a wavelength of 600 nm. The pulse train from the amplifier was split into two pulse trains. One beam was used as pump which excited the sample. The delay line on the translation stage was inserted in one of the two beams, which is called as probe beam. Both pulses pass through the lenses

of focal length of 15 cm and 50 cm with different initial diameters of ~4 mm (pump beam) and ~2 mm (probe beam) respectively, and they were focused on the sample. The spatial overlap of the two pulses was aligned into a NLO sample. We strictly followed the ratio of pump to probe intensities to be >20. A chopper was utilized to modulate the pump beam at 109 Hz and the differential probe transmittance from the sample was recorded by a photodiode (SM05R/M, Thorlabs) which is in the combination of a lock-in amplifier (7265, Signal Recovery). The polarization of pump/probe beams was perpendicular to avoid coherent artefacts. The translation stage was controlled by the ESP motion controller. Both lock-in-amplifier and motion controllers were interfaced with LabView program. Autocorrelation technique was utilized for the optimizing experimental setup for getting the zero delay which provided the spatial and temporal overlap of the beams meeting at the sample.

III. RESULTS AND DISCUSSION

A. TEM, HRTEM and SAED characterizations of Si colloids

We have performed systematic studies of colloidal Si NPs produced by single line laser ablation[34] of highly doped Si targets (Boron concentration was ~10^{18}/cc) immersed in four liquids (acetone, water, DCM and chloroform). To avoid ambiguity, Si NPs fabricated through single line ablation in acetone, water, DCM, and chloroform were labeled as SiNP1, SiNP2, SiNP3 and SiNP4, respectively. The concentration/distribution of NPs and their crystalline nature were estimated from TEM and SAED measurements. Figure 1 shows the TEM images of Si NPs produced in SiNP1 [figure 1(a)] and SiNP2 [figure 1(c)] and insets in these figures show the corresponding size histogram distribution of NPs which were fitted with Gaussian curves. The mean diameter was determined to be ~9.5 nm for SiNP1 in acetone and ~37 nm for SiNP2 in water. Figures 1(b)

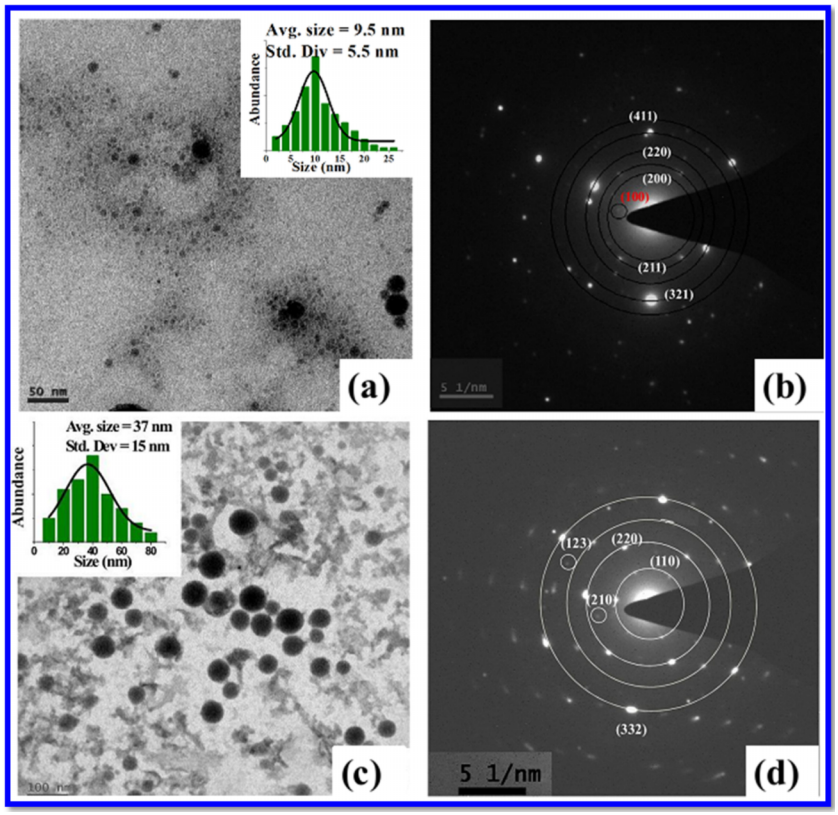

FIG. 1. TEM images of **(a)** SiNP1 and **(c)** SiNP2 and insets of **(a)** and **(c)** depict the NPs distribution. SAED spectra of **(b)** SiNP1 and **(d)** SiNP2.[41] Copyright OSA. Reproduced with permission from Optical Society of America, USA.

and 1(d) illustrate SAED patterns of SiNP1 and SiNP2 which confirmed poly-crystalline nature of the fabricated Si Nps. The corresponding five planes have been considered for estimating the interplanar spacing of 3.35 Å, 2.69 Å, 2.35 Å, 1.77 Å and 1.57 Å which agreed well with pure Si (200), (211), (220), (321) and (411) crystal planes of cubic phase in the case of SiNP1. Moreover, one of the crystal planes with interplanar spacing of 5.72 Å corresponds to Si (100) crystal planes with hexagonal phase. For the case of SiNP2, the interplanar spacings estimated from crystal planes were 2.6 Å and 1.64 Å, which matched well with SiO_2 cubic crystal planes of (110) and (210). In addition, two more planes [(220) and (332)] identified were corresponding to the 'd' values being 2.35 Å and 1.42 Å [similar to pure Si with cubic phase]. Thus, from the SAED pattern, we confirmed that pure Si NPs and Si/SiO_2 NPs have been generated in cases of SiNP1 and SiNP2, respectively.

TEM data of the fabricated Si NPs in DCM (SiNP3) and chloroform (SiNP4) are presented in figures 2(a) and 2(c), respectively, and insets depict the size distribution histograms. As observed from the TEM images of 2(a) and 2(c), the NPs were aggregated spheres covered with thin layers of carbon. The average sizes for SiNP3 and SiNP4 were ~45 nm and ~42 nm, respectively. Figures 2(b) and 2(d) represent SAED patterns of SiNP3 and SiNP4, respectively. The NPs in SiNP3 depicted polycrystalline phase (cubic phase) with interplanar spacings of 3.34 Å, 2.72 Å, 2.33 Å, 1.92 Å, 1.49 Å, and 1.31 Å corresponding to crystalline Miller planes of Si (200), (211), (220), (222), (420) and (134), respectively. Similarly, SAED ring pattern for SiNP4 resemble Si (200), (211), (220), and (411) and their corresponding 'd' values were found to be 3.34 Å, 2.72 Å, 2.33 Å, and 1.57 Å. Moreover, other diffraction rings with lattice spacings for both the cases (SiNP3 and SiNP4) were 0.73 Å and 0.68 Å and are ascribed to be the 'd' values of Carbon (C) (422) and (431) planes, respectively. From these TEM and SAED studies we are able to conclude that we have synthesized pure Si NPs in acetone (SiNP1), Si/SiO_2 NPs in water (SiNP2), Si NPs covered by

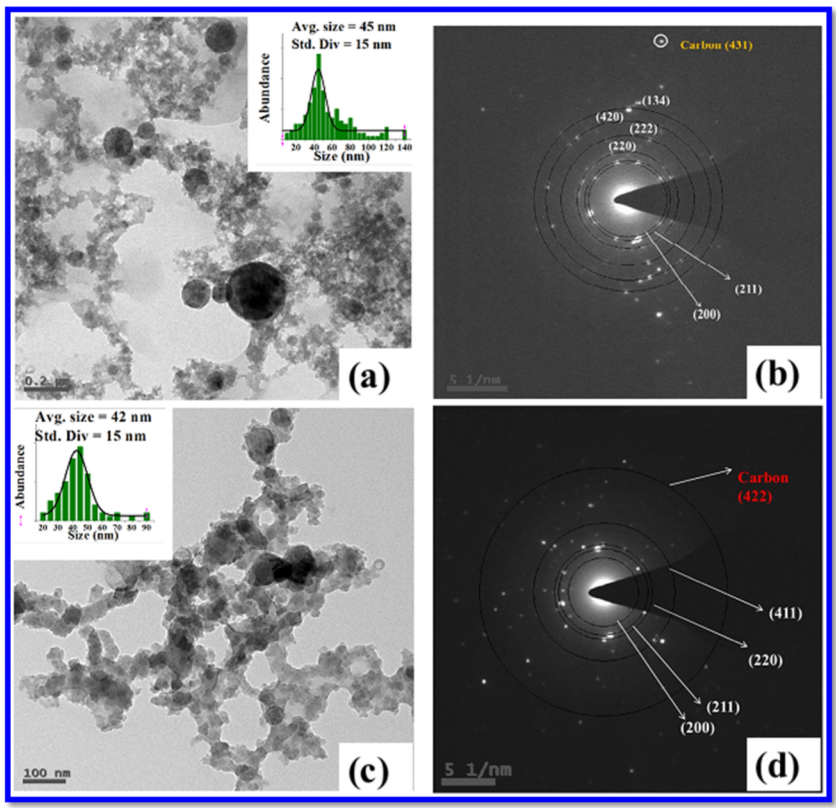

FIG. 2. TEM images of **(a)** SiNP3 and **(c)** SiNP4 and insets of **(a)** and **(c)** depict the NPs distribution. SAED patterns of **(b)** SiNP3 and **(d)** SiNP4.[41] Copyright OSA. Reproduced with permission from Optical Society of America, USA.

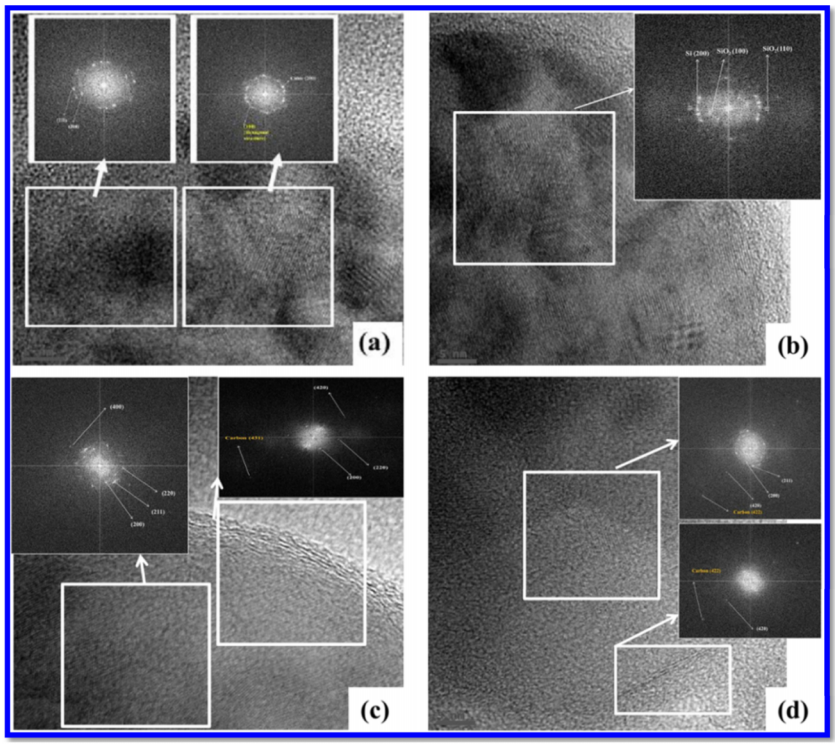

FIG. 3. HRTEM images of (a) SiNP1 (b) SiNP2 (c) SiNP3 and **(d)** SiNP4 illustrating the view of lattice planes observed at different characteristic separations.[41] Insets show the numerical electronic diffraction pattern of HRTEM images which confirmed the planes of Si, Si/SiO_2, Si-C and Si-C lattice sets, respectively. Copyright OSA. Reproduced with permission from Optical Society of America, USA.

carbon matrix in both DCM (SiNP3) and chloroform (SiNP4). These conclusions, drawn from the above characterizations, were additionally supported by high resolution TEM (HRTEM) and Raman spectral data of the colloidal Si NPs, as discussed below.

Figures 3(a)–3(d) illustrate the HRTEM images of SiNP1-SiNP4 and inset shows the FFT of HRTEM images. The FFT patterns of lattice planes from HRTEM correlate the SAED patterns. For SiNP1 [figure 3(a)], the interplanar spacings of lattice planes, 5.71 Å and 3.34 Å were attributed to the approximate lattice spacings of hexagonal phase pure Si (100) plane and cubic phase of pure Si (200), respectively. In the case of water (SiNP2), the measured inter planar separations of 4.7 Å and 2.64 Å were in good agreement with SiO_2 (100) and (110) planes, respectively, and 3.3 Å corresponding to pure Si (200) is shown in figure 3(b). For SiNP3 and SiNP4 prepared in chlorine based solvents [(figure 3(c) and figure 3(d)], the 'd' values obtained from the FFT of HRTEM images were 0.73 Å (SiNP3) and 0.68 Å (SiNP4) belonging to C (422) and (431) planes in both cases along with Si planes. This characterization validated the formation of Si NPs in carbon matrix.

B. Raman, UV-Vis absorption and PL studies of Si NPs

Figure 4 depicts the Raman spectra of Si NPs produced in SiNP1-SiNP4 with 532 nm excitation. The position and broadening of the crystalline peak determines the nature of Si NPs. The peak position decides the crystalline nature and broadening reflects the size effects. A peak near ~515 cm^{-1} was detected for all the samples confirming the crystalline nature of Si NPs while the peak position of bulk Si (near 520.8 cm^{-1}) was also recorded as a reference for observing the shift. The shift observed (to lower wave numbers) and broadening of the TO phonon line from the NPs is usually attributed to the phonon quantum confinement effect. However, in our case most of the generated NPs were larger in size (compared to Bohr exciton radius) indicating that the confinement effects are not significant. Strain in these NPs is one of the possible reasons for the observed large

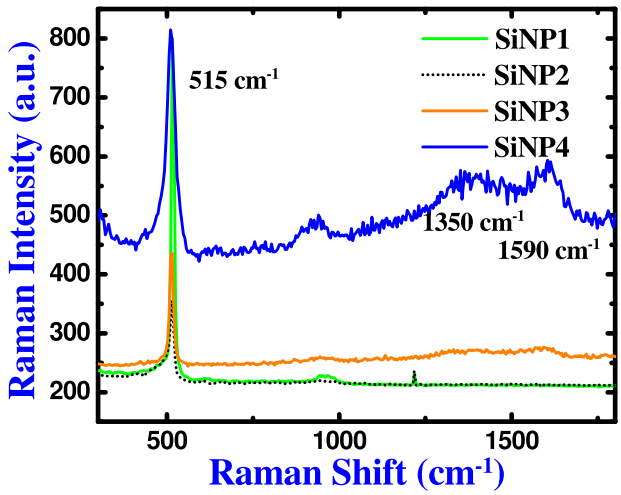

FIG. 4. Raman spectra of Si NPs in (i) SiNP1 (ii) SiNP2 (iii) SiNP3 (iv) SiNP4 depicting a crystalline peak near 515 cm^{-1}. Two carbon bands were observed at 1350 cm^{-1} and 1590 cm^{-1} in both SiNC3 and SiNC4.

shift in the peak position. If the strain was non-uniform it could create a tail extending to lower energy which might account for some of the structure. Other than that, two peaks were also identified near 1350 cm^{-1} (D-band) and 1605 cm^{-1} (G-band) in both SiNP3 and SiNP4, which confirmed the presence of carbon along with Si NPs. These studies confirm the formation of Si-C nanocomposites in SiNP3 and SiNP4.

The Si NPs obtained through ULAL possessed broad absorption band in UV–near infrared (NIR) region of the electromagnetic spectrum. The absorption band was observed in the 300-800 nm range for all samples, though with different intensities. Figures 5(a) and 5(b) illustrate UV–Visible absorption and PL spectra of colloidal Si NPs in different liquids, respectively. Careful observation of the absorption spectra [data presented in figure 5(a)] revealed the presence of an additional band with little wavelength shift (328 nm, 282 nm and 274 nm) in the cases of SiNP1, SiNP3 and SiNP4 while no such band was observed in the case SiNP2 (water). The liquid properties could have played a significant role for this wavelength shift, which might not be due to the differences in sizes of NPs. The sharp absorption peak observed in acetone (near 328 nm) could possibly be attributed to impurities in the solvent. However, further detailed studies are essential to identify the exact reason for this. The absorption spectrum recorded in water agrees well with previous reports.[32] Figure 5(b) represents the PL spectra of colloidal Si NPs deposited on glass slides. All the

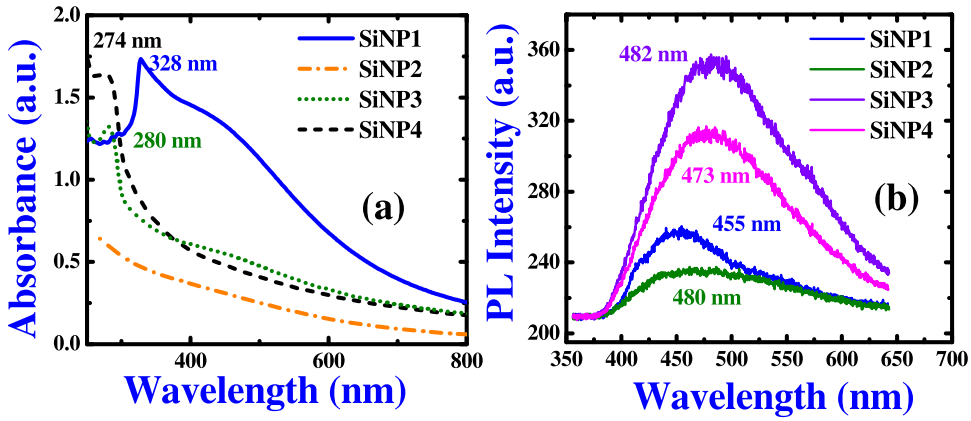

FIG. 5. **(a)** UV-Vis absorption spectra and **(b)** PL spectra of SiNPs prepared through ps laser ablation in acetone (SiNP1), water (SiNP2), DCM (SiNP3) and chloroform (SiNP4).

samples illustrated a significant amount of PL, with peaks observed near 455 nm, 480 nm, 482 nm and 473 nm for SiNP1, SiNP2, SiNP3 and SiNP4, respectively. Furthermore, we have verified that the PL spectra was indeed from the Si NPs since the PL peak position at 570 nm of glass slide was taken as reference for quantifying the PL peak attributed to Si NPs. As observed from results of PL, the position of PL peak was not overtly dependent on the size of NPs. But different peak positions were obtained for different samples, which could be due to usage of different liquid media resulting in different passivation states such as SiO_2, SiC etc. There are, at least, four main mechanisms proposed for the observed blue PL from a variety of Si NPs: (a) due to oxide-related defects (b) due to quantum confinement effects (iii) due to a combination of quantum confinement effects and surface states (iv) due to direction band gap emissions.[76] Yang et al.[76] reported the PL of laser ablated Si NPs (2-10 nm size) in the 400-450 nm spectral region which shifted to the red region on annealing. The PL of generated Si NPs in different liquid media have demonstrated different peak positions due to the interaction of ultrafast laser beam with liquid media, possibly producing carbon byproducts. These carbon byproducts could perhaps occupy position on the surface of the NP resulting in formation of Si–C material, allowing changes in the electronic energy levels for the system. In our case there could also be the effect of surface states resulting in the observed PL. We also do not rule out the possibility of oxidation effects. Recently, Intartaglia et al.[77] reported that the interaction takes place between laser and solvent molecule and this influences the PL of Si NPs produced by laser ablation. Liquid media was found to affect the microstructure of the obtained SiNPs and on the optical properties of the colloidal solution. SiNPs with high pressure structure (s.g. *Fm3m*) and diamond-like structure (s.g. *Fd3m*) were observed for the case of ablation in water. For the case of toluene, Si-NPs and SiC-NPs with moissanite 3C phase were observed. PL studies demonstrated that the water-synthesized SiNPs presented very specific blue-green emission. Laser synthesis in toluene solvent led to the formation of Si-NPs embedded in a graphitic carbon–polymer composite originating from the interaction of the toluene molecules with the UV photons (ablation source).[77] Intartaglia et al.[28] again obtained Si colloids prepared at higher fluence where they observed a mean size of ~65 nm (sizes varying from 10 nm to 120 nm). They argue that due to large sized NPs (compared to the Bohr exciton radius of 4.9 nm) they were considered to be in a weak confinement regime, with a lower energy band gap and, therefore, observed a red-shifted emission. Abderaffi et al.[78] studied ns pulse ablated Si NPs in isopropanol (~40 nm mean size) and observed a broad PL peak in the vicinity of 500 nm. In their case the PL peak was located near 470 nm for the NPs prepared with lower energies similar to the peak observed (near 480 nm) in the present studies. Similarly, Alkis et al.[27] obtained Si NPs in the 5-100 nm size range with PL near 500 nm while fragmentation studies revealed smaller sized particles and blue shifted PL. In the present case we believe that the PL characteristics observed could possibly be attributed to (a) surface effects of the NPs (It could perhaps be from SiO_2 or from the C related species on the surface, or even a hybrid transition involving the Si core and a surface species) and/or (b) aging effects since the emission spectra were collected few weeks post ablation process. Further detailed studies are warranted to identify the exact mechanisms.

C. FESEM and Raman characterization of Si NSs

In our experiments we could also produce nanostructures (NSs) on the Si substrates simultaneously along with colloidal Si NPs. In this context, the generated NSs in different liquid media such as acetone, water, DCM and chloroform were labeled as SiNS1, SiNS2, SiNS3 and SiNS4, respectively. The Si surface area exposed to laser ablation in liquids acquired LIPSS, which depended on the liquid media and number of pulses. Here, we attempted changing the liquid media to obtain NSs on Si substrate using constant number of laser pulses. The FESEM images of Si substrates after the ablation using in various liquids are illustrated in figure 6. The morphological characterization of ablated Si in acetone [SiNS1- figure 6(a)] and water [SiNS2- figure 6(b)] demonstrated the formation of HSFL with period of ~140 nm and ~105 nm, respectively, as evident from the FESEM images. As per the data presented in figure 6, average particle sizes of ~40 nm (SiNS1) and ~55 nm (SiNS2) NPs were also observed on the top of each NS. Figures 6(c) and 6(d) demonstrate FESEM images of the Si surface which was ablated in DCM (SiNP3) and chloroform

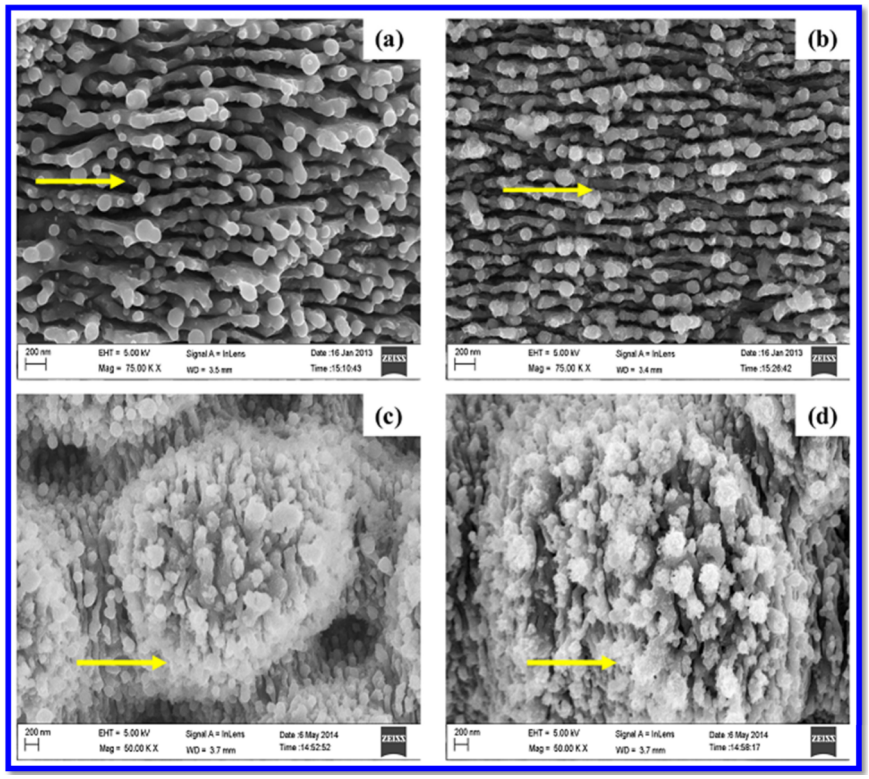

FIG. 6. FESEM images of laser induced surface structures that were fabricated on Si substrate by ps laser ablation of bulk Si in liquid media (a) SiNS1 **(b)** SiNS2 **(c)** SiNS3 and **(d)** SiNS4. The arrow indicates the direction of laser polarization.

(SiNP4), respectively. In these liquids the structures formed were random in nature and dissimilar to the LIPSS. These structures might have been formed due to differences in the liquid properties such as viscosity and surface tension. Moreover, there was aggregation of NPs with cloud shape layer forming on the top of the randomly oriented structures synthesized on upper part of the Si surface while no cloud type structures were observed underneath the Si surface. This could be a carbon layer which was later confirmed by Raman spectroscopy. There could, possibly, be two reasons for the formation of aggregating NPs with cloud shape layer: (a) short-term interaction of generated Si ions in the plasma plume with the C ions in the liquid medium resulted in formation of Si-C NPs[79] (b) the reactivity of laser beam with carbon in surrounding liquid to form carbon products like a layer around the Si NP. The orientation of these surface structures was parallel to the polarization of input laser beam in SiNS1 and SiNS2, and perpendicular to the polarization of input laser beam in SiNS3 and SiNS4. However, further detailed investigation is necessary to understand this intriguing behavior. Figure 7 represents the Raman spectra of NSs on Si Substrates generated by ULA of Si in different liquids of acetone (SiNS1), water (SiNS2), DCM (SiNS3) and chloroform (SiNS4). Several peaks were detected at 515 cm^{-1}, 516 cm^{-1}, 519 cm^{-1} and 515 cm^{-1} which confirmed the formation of nano crystalline Si and another peak was observed near 483 cm^{-1} demonstrating the amorphization of substrates. As seen from the Raman spectra, two peaks were observed at 1350 cm^{-1} (D-band) and 1592 cm^{-1} (G-band) in both SiNS3 and SiNP4 and these confirmed that carbon was present along with Si NPs.

D. NLO studies of Si colloids

We have investigated the third order nonlinearity of laser fabricated Si NPs in different liquid media (acetone, water, DCM and chloroform) by Z-scan technique with fs oscillator pulses at a wavelength of 680 nm. Figure 8 illustrates the open aperture (OA) Z-scan data of (a) Si NPs in

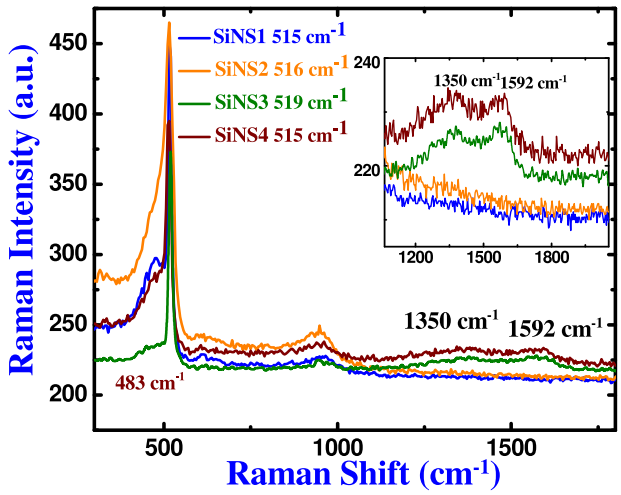

FIG. 7. Raman spectra of nanostructures on the Si substrates illustrating an amorphous peak near 483 cm^{-1} and asymmetric crystalline peak at (i) 515 cm^{-1} in SiNS1 (ii) 516 cm^{-1} in SiNS2 (iii) 519 cm^{-1} in SiNS3 and (iv) 515 cm^{-1} in SiNS4. Two carbon peaks at 1350 cm^{-1} and 1592 cm^{-1} were observed in SiNS3 and SiNS4.

acetone (b) Si/SiO_2 NPs in water (c) Si-C NPs in DCM and (d) Si-C NPs in chloroform, recorded at a peak intensity of ~0.38 GW/cm^2. As observed from the obtained OA data, all the NPs (except Si/SiO_2 NPs) demonstrated a dip in the transmittance when the sample reached the focal point and the dip designates pure RSA. To analyze the OA data, we fitted the RSA signature with standard transmittance equation[80] which contains 2PA coefficient (β) term and the estimated values of 'β' were ~1.9×10^{-11}cm/W, ~6×10^{-11}cm/W and ~6.2×10^{-11}cm/W for Si NPs in acetone, Si-C NPs in DCM and Si-C NPs in chloroform, respectively. The presence of nonlinear absorption at the

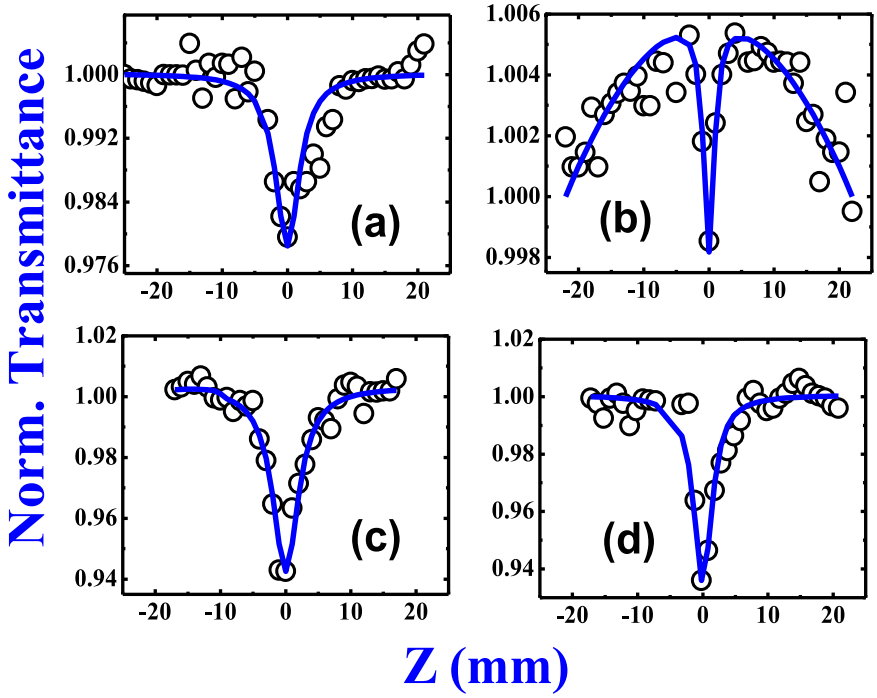

FIG. 8. Open aperture Z-scan data of **(a)** Si NPs in acetone (SiNP1) **(b)** Si/SiO_2 NPs in water (SiNP2) **(c)** Si-C in DCM (SiNP3) and **(d)** Si-C NPs in chloroform (SiNP4) recorded with peak intensity of ~0.38 GW/cm^2 at 680 nm wavelength using ~150 fs pulses. Open circles represent the experimental data while solid lines are theoretical fits.

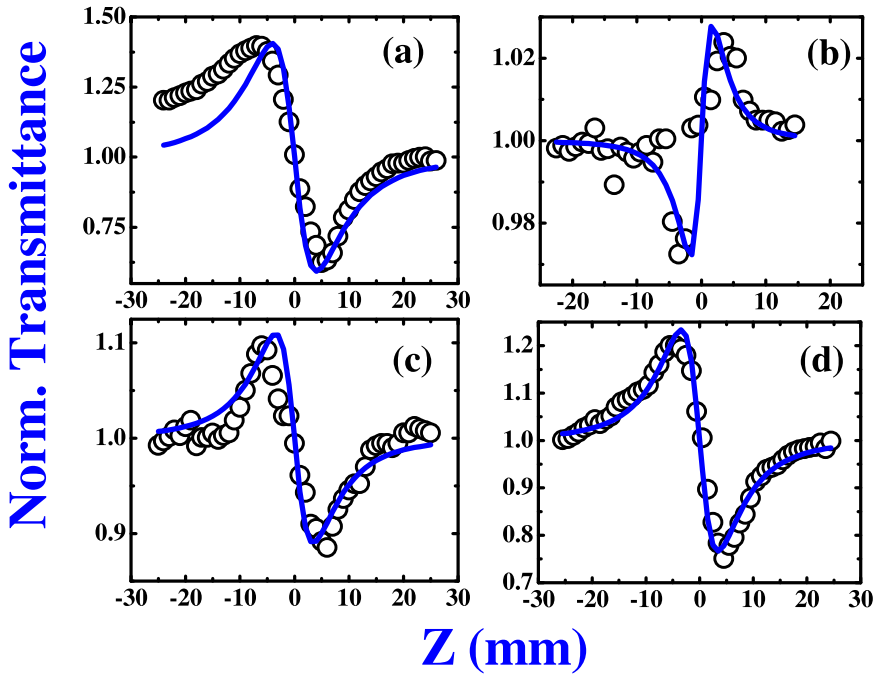

FIG. 9. Closed aperture Z-scan data of **(a)** Si NPs in acetone (SiNP1) **(b)** Si/SiO_2 NPs in water (SiNP2) **(c)** Si-C in DCM (SiNP3) and **(d)** Si-C NPs in chloroform (SiNP4) recorded with peak intensity of ~0.1 GW/cm^2 at 680 nm wavelength using ~150 fs pulses. Open circles represent the experimental data while solid lines are theoretical fits.

excitation of 680 nm could be based on the inter band transitions which is related to the strong linear absorption near 300 nm. On the other hand, Si/SiO_2 NPs in water illustrated a switching behavior (RSA in SA) and the data was fitted with the combination of saturation intensity and nonlinear absorption coefficient (or 2PA) to follow the standard procedure. The switching behavior could be due to broad absorption band in the linear absorption spectra which covers the excitation wavelength of 680 nm. The estimated values of saturation intensity (I_S) and β were ~1.2×10^4 W/cm^2 and ~2×10^{-10} cm/W, respectively. Figure 9 shows the closed aperture Z-scan data of (a) Si NPs in acetone (b) Si/SiO_2 NPs in water (c) Si-C NPs in DCM and (d) Si-C NPs in chloroform, recorded at a peak intensity of 0.1 GW/cm^2. A few researchers have reported that Si NPs in different media exhibiting stronger nonlinearities.[45,81,82] Our recorded data demonstrated a peak-valley signature which confirmed that all the NPs (except Si/SiO_2 NPs) illustrated self-defocusing behavior while Si/SiO_2 NPs demonstrated self-focusing behavior (indicating negative and positive nonlinearities). The values of n_2 obtained from the fitted data using standard equation[78] were ~8.2×10^{-13} cm^2/W, ~4.9×10^{-14} cm^2/W, ~1.9×10^{-13} cm^2/W and ~4×10^{-13} cm^2/W and, and the magnitudes of $|\chi^{(3)}|$ values estimated were ~1.9×10^{-14} e.s.u., ~2×10^{-13} e.s.u., ~6.7×10^{-14} e.s.u. and ~7.1×10^{-14} e.s.u. for Si NPs, Si/SiO_2 NPs, Si-C NPs in DCM and Si-C NPs in chloroform, respectively. Moreover, the observed strong nonlinearity in these NPs could be due to combination of electronic nonlinearity and thermal nonlinearity since large numbers of pulses were incident on the sample (80 MHz). The solvent nonlinearity was negligible compared to that of NPs. There could be an error of ±10% in the values of NLO coefficients cited above. The errors arise from (a) fluctuations in the input laser pulses resulting in noisy experimental data (b) fitting procedures used (c) estimation of the beam waist ($2\omega_o$) at focus leading to errors in the estimation of peak input intensities etc.

E. Pump-probe studies of Si NPs

Figure 10 illustrates the pump-probe data for (a) pure Si NPs in acetone (b) Si/SiO_2 NPs in water (c) Si-C NPs in DCM and (d) Si-C NPs in chloroform obtained from degenerate pump-probe measurements at 600 nm with ~70 fs pulses. Typically, pump and probe intensities used were

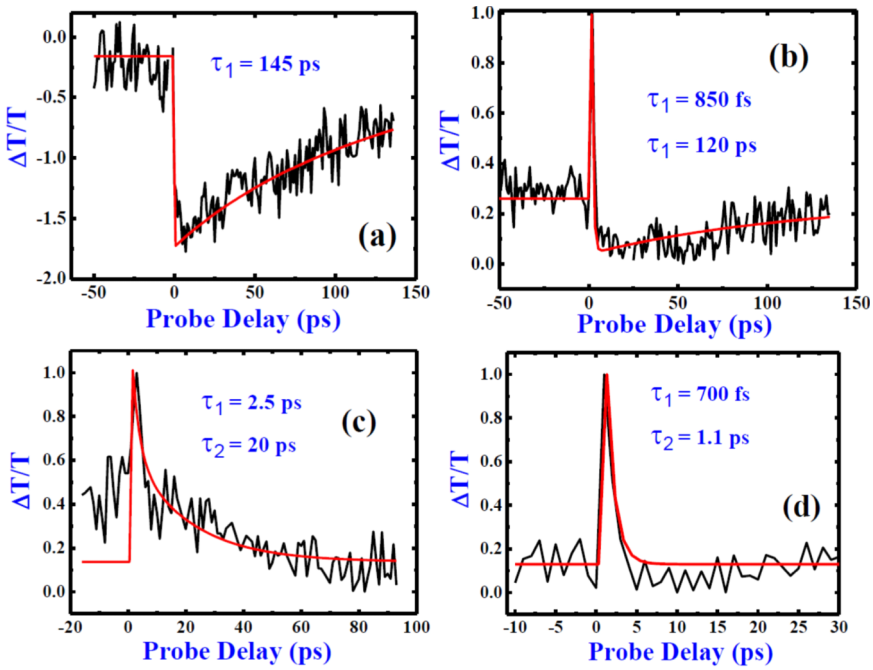

FIG. 10. Pump-probe dynamics of **(a)** Si NPs in acetone (SiNP1) **(b)** Si/SiO_2 NPs in water (SiNP2) **(c)** Si-C in DCM (SiNP3) and **(d)** Si-C NPs in chloroform (SiNP4) recorded at an excitation wavelength of 600 nm wavelength with ~70 fs pulses.[41] Copyright OSA. Reproduced with permission from Optical Society of America, USA.

~200 GW/cm^2 and ~5 GW/cm^2, respectively. It can be noticed that the differential probe transmission was photo induced absorption (negative transmission) for pure Si NPs in acetone [data shown in figure 10(a)]. Here, the excitation wave length was nearly half of sample absorption band (~328 nm) and other three samples showed photo bleaching curves in figures 10(b)–10(d) since the excitation wavelength is more towards the broad absorption band than other peaks (no peak for Si/SiO_2, 282 nm for Si-C in DCM and 274 nm for Si-C NPs in chloroform). Single exponential was used to fit the photo induced absorption curve in figure 10(a). Double exponential equation was utilized to fit the other experimental data and two life times were acquired from fits for all the other samples. The obtained lifetimes were τ_1 = ~145 ps for pure Si NPs in acetone, τ_1 = ~850 fs and τ_2 = ~122 ps for Si/SiO_2 NPs in water, τ_1 = ~2.5 ps and τ_2 = ~20 ps for Si-C NPs in DCM and τ_1 = ~700 fs and τ_2 = ~1.1 ps for Si-C NPs in chloroform. The long decay time of τ_1 = ~145 ps demonstrated by pure Si NPs in acetone [figure 10(a)] could be tentatively assigned to the phonon-phonon relaxations. The shorter life times of τ_1 = ~850 fs [figure 10(b)] and τ_1 = ~700 fs [figure 10(d)] could possibly be assigned to the electron-electron relaxations and, τ_1 = ~2.5 ps [figure 10(c)] can possibly be attributed to the electron-phonon relaxation time. The second decay time of τ_2 = ~122 ps [figure 10(b)] obtained could be due to phonon-phonon relaxation (the possibility of non-radiative transitions). Moreover, τ_2 = ~20 ps [figure 10(c) and τ_2 = ~1.1 ps [figure 10(d)] are assigned to the electron-phonon relaxation and electron-electron relaxations, respectively. In the present case we had fitted single/double exponential decay fits to the experimental data based on the χ^2 values and the number of available data points.

Si NPs demonstrating longer lifetimes are usually influenced by the size of NPs.[83] These studies will be extended in near future, to comprehend the correlations between the emission properties and ultrafast dynamics.[84] Wang et al.[84] performed optical spectroscopic studies to understand the underlying mechanism of tunable PL (450-520 nm) in 2-3 nm Si quantum dots whose surfaces were modified. Further, their time-resolved studies revealed ultrashort lifetime components of 1.8 ps, 34 ps and 190 ps for Di–Si QDs and four lifetime components of 1.2 ps, 9 ps, 100 ps and 1 ns for Ca–Si QDs, which are best attributed to the non-radiative excited-state processes. It has also been confirmed from several studies that[85] silicon NCs typically exhibit bi-exponential decay

kinetics with a fast decay (<1 ps) frequently attributed to exciton trapping and/or thermalization and the slower decay component (30-100 ps) being attributed to primary recombination pathways. In the present case our intention was to understand the qualitative dynamics of the produced Si NPs when excited with ultrashort laser pulses. Further detailed studies are required to assign the observed lifetimes to different physical mechanisms.

The technique of laser ablation in liquids[28,36] offers several advantages for preparing Si NPs and nanostructures. Intartaglia et al.[32] have demonstrated gram per hour yield of ultra-small SiNPs using ps pulses. They developed an original model based on the *in-situ* ablation/photo-fragmentation physical process. The model successfully explained the experimental productivity findings in their case. Bagga et al.[86] have demonstrated fabrication of protein-functionalized luminescent Si NPs based on laser ablation of Si in an aqueous solution of *Staphylococcus aureus* protein A. Such NPs find applications in real-time cell labeling, cell staining and controlled drug delivery.[86] Furthermore, Intartaglia et al.[87] achieved bio-functionalized Si quantum dots using this method suggesting the strong potential of preparing a variety of Si NPs for applications (e.g. nucleic acid vector delivery). Krillin et al.[88] recently demonstrated the usage of SI NPs in optical coherence tomography wherein the NPs were created in water using laser ablation technique. The potential of those fabricated Si NPs as a contrasting agent for optical coherence tomography was investigated by performing experiments with agarose gel phantoms. Further, Li et al.[89] have very recently demonstrated that the production rate of SI NPs could be enhanced (by ~2.6 times) by shaping the input ultrashort laser pulses used. The production-rate enhancement was mainly attributed to high photon absorption efficiency. Chefenov et al. recently produced Si NPs (4-6 nm) with fs pulses and observed PL in the 500-600 nm spectral window.

IV. CONCLUSIONS

In summary, this study offered a comprehensive look at the elemental composition and size of Si NPs and Si NSs in four different liquid media achieved through ps ablation technique. In the interaction of ultrafast laser with Si in acetone and water, we found HSFL structures with a spacing of ~140 nm in SiNS1 and ~105 nm in SiNS2, while NPs with characteristic size of ~9.5 nm (pure Si NPs) and ~20 nm (Si/SiO_2 NPs) were observed in liquids acetone and water, respectively. Additionally, a random cloud like submicron structures (SiNS3 and SiNS4) were found in chloride based liquid experiment and aggregated Si NPs in carbon matrix with mean size 45 nm and 42 nm in DCM (Si-C NPs) and chloroform (Si-C NPs). The elemental composition of NPs and NSs was confirmed by SAED, HRTEM and Raman spectroscopy. Formation of LIPSS and NPs in liquids could be ascribed due to various mechanisms such as nonlinear effects, generation of mechanical pressures, interference effects etc. Fs NLO properties of four colloids have been studied and we found that 2PA phenomenon has contributed to the third-order nonlinearity. The excited-state dynamics in colloidal Si NPs, investigated using degenerate fs pump− probe technique, were observed to possess double-exponential decay constants with time scales in both fs and ps domains. The observation of short-lived excited-state lifetime in the range of 700-850 fs could be due to electron-electron relaxation and long lived excited state lifetime in the range of 1.1-145 ps could be due to electron-phonon relaxation and phonon-phonon relaxations.

ACKNOWLEDGMENTS

Authors acknowledge DRDO, India for the continued financial support and also thank **UPE-II,** University of Hyderabad for partial financial support. APP thanks CSIR for the Emeritus Scientist award. Authors thanks Centre for Nanotechnology, UoH for assistance in recording the TEM data.

[1] T. Erogbogbo, K.T. Yong, I. Roy, R. Hu, W.C. Law, W. Zhao, H. Ding, F. Wu, R. Kumar, M.T. Swihart, and P.N. Prasad, ACS Nano **5**, 413 (2011).
[2] Z. F. Li and E. Ruckenstein, Nano Lett. **4**, 8 (2004).
[3] G. Wang, S. T. Yau, K. Mantey, and M. H. Nayfeh, Opt. Commun. **281**, 1765 (2008).

[4] G. Belomoin, J. Therrien, A. Smith, S. Rao, R. Twesten, S. Chaieb, M. H. Nayfeh, L. Wagner, and L. Mitas, Appl. Phys. Lett. **80**, 841 (2002).
[5] J.H. Park, L. Gu, G. von Maltzahn, E. Ruoslahti, S.N. Bhatia, and M.J. Sailor, Nature Mater. **8**, 331 (2009).
[6] G. Ledoux, J. Gong, F. Huisken, O. Guillois, and C. Reynaud, Appl. Phys. Lett. **80**, 4834 (2002).
[7] X.Y. Chen, Y.F. Lu, Y.H. Wu, B.J. Cho, M.H. Liu, D.Y. Dai, and W.D. Song, J. Appl. Phys. **93**, 6311 (2003).
[8] W. J. I. DeBenedetti, S.-K. Chiu, M. C. Radlinger, J. R. Ellison, A. B. Manhat, Z. J. Zhang, J. Shi, and M. A. Goforth, J. Phys. Chem. C **119**, 9595 (2015).
[9] S. Godefroo, M. Hayne, M. Jivanescu, A. Stesmans, M. Zacharias, O. I. Lebedev, G. Van Tendeloo, and V. V. Moshchalkov, Nat. Nanotechnol. **3**, 174 (2008).
[10] K. Dohnalova, A. N. Poddubny, A. A. Prokofiev, W. de Boer, C. P. Umesh, J. M. J Paulusse, H. Zuilhof, and T. Gregorkiewicz, Light Sci. Appl. **2**, 1 (2013).
[11] Y. Kanemitsu, Phys. Rev. B **49**, 16845 (1994).
[12] D. Mariotti, S. Mitra, and V. Svrcek, Nanoscale **5**, 1385 (2013).
[13] S.M. Liu, J. Nanosci. Nanotechnol. **8**, 1110 (2008).
[14] W. D. A. M de Boer, D. Timmerman, K. Dohnalova, I. N Yassievich, H. Zhang, W. J. Buma, and T. Gregorkiewicz, Nat. Nanotechnol. **5**, 878 (2010).
[15] C.-C. Tu, L. Tang, J. Huang, A. Voutsas, and L.Y. Lin, Opt. Exp. **18**, 21622 (2010).
[16] J. Choi, Wang N. S, and V. Reipa, Bioconj. Chem. **19**, 680 (2008).
[17] Z. F Li and E. Ruckenstein, Nano Lett. **4**, 1463 (2004).
[18] I. A. Rahman and V. Padavettan, J. Nanomat. **2012**, 132424 (2012).
[19] I. Alghoraibi and A. A. Ahmad, Int. J. Chem. Tech. Res. **6**, 871 (2014).
[20] K. J. Klabunde, Y.-X. Li, and B.-J. Tan, Chem. Mater. **3**, 30 (1991).
[21] K. J. Klabunde and G. C. Cardenas-Trivino, in *Active Metals*, edited by A. Fürstner (VCH, Weinheim, 1996), pp. 237–278.
[22] N. G. Semaltianos, S. Logothetidis, W. Perrie, S. Romani, R. J. Potter, S. P. Edwardson, P. French, M. Sharp, G. Dearden, and K. G. Watkins, J. Nanopart. Res. **12**, 573 (2010).
[23] P. Blandin, K.A. Maximova, M. B. Gongalsky, J.F. Sanchez-Royo, V.S. Chirvony, M. Sentis, V. Y. Timoshenko, and A.V. Kabashin, J. Mater. Chem. B **1**, 2489 (2013).
[24] D. Tan, Z. Ma, B. Xu, Y. Dai, G. Ma, M. He, Z. Jin, and J. Qiu, Phys. Chem. Chem. Phys. **13**, 20255 (2011).
[25] E. V. Barmina, C. Fotakis, P. A. Loukakos, E. Stratakis, and G. A. Shafeev, Appl. Phys. A **117**, 359 (2014).
[26] D. Rioux, M. Laferrière, A. Douplik, D. Shah, L. Lilge, A.V. Kabashin, and M.M. Meunier, J. Biomed. Opt. **14**, 021010 (2009).
[27] S. Alkis, A. K. Okyay, and B. Ortaç, J. Phys. Chem. C **116**, 3432 (2012).
[28] R. Intartaglia, K. Bagga, M. Scotto, A. Diaspro, and F. Brandi, Opt. Mater. Express **2**, 510 (2012).
[29] R. Intartaglia, K. Bagga, F. Brandi, G. Das, A. Genovese, E. Di Fabrizio, and A. Diaspro, J. Phys. Chem. C **115**, 5102–510 (2011).
[30] H. Liu, F. Chen, X. Wang, Q. Yang, H. Bian, J. Si, and X. Hou, Thin Solid Films **518**, 5188 (2010).
[31] S. Hamad, G. Krishna Podagatlapalli, V. S. Vendamani, S. V. S. Nageswara Rao, A. P. Pathak, S. P. Tewari, and S. Venugopal Rao, J. Phys. Chem. C **118**, 7139 (2014).
[32] R. Intartaglia, K. Bagga, and F. Brandi, Opt. Express **22**(3), 3117 (2014).
[33] G. Krishna Podagatlapalli, S. Hamad, S. Sreedhar, S. P. Tewari, and S. Venugopal Rao, Chem. Phys. Lett. **530**, 93 (2012).
[34] G. Krishna Podagatlapalli, S. Hamad, S. P. Tewari, S. Sreedhar, M. D. Prasad, and S. Venugopal Rao, J. Appl. Phys. **113**, 073106 (2013).
[35] S. Hamad, G. Krishna Podagatlapalli, M. A. Mohiddon, and S. Venugopal Rao, Appl. Phys. Lett. **104**, 263104 (2014).
[36] S. Venugopal Rao, G. Krishna Podagatlapalli, and S. Hamad, J. Nanosci. Nanotech. **14**, 1364 (2014).
[37] G. Krishna Podagatlapalli, S. Hamad, M. A. Mohiddon, and S. Venugopal Rao, Appl. Surf. Sci. **303**, 217 (2014).
[38] S. Hamad, G. Krishna Podagatlapalli, M. A. Mohiddon, and S. Venugopal Rao, Chem. Phys. Lett. **621**, 553 (2015).
[39] G. Krishna Podagatlapalli, S. Hamad, Md. Ahamad Mohiddon, and S. Venugopal Rao, Las. Phys. Lett. **12**, 036003 (2015).
[40] G. Krishna Podagatlapalli, S. Hamad, and S. Venugopal Rao, J. Phys. Chem. C **119**, 16972-16983 (2015).
[41] S. Hamad, G. Krishna Podagatlapalli, S. V. S. Nageswara Rao, A. P. Pathak, and S. Venugopal Rao, in *12th International Conference on Fiber Optics and Photonics*, OSA Technical Digest (online) (Optical Society of America, 2014), paper T3A.48. https://www.osapublishing.org/abstract.cfm?uri=Photonics-2014-T3A.48.
[42] O. Varlamova, F. Costache, J. Reif, and M. Bestehorn, Appl. Surf. Sci. **252**, 4702 (2006).
[43] J. E. Sipe, J. F. Young, J. S. Preston, and H. M. Vandriel, Phys. Rev. B **27**, 1141 (1983).
[44] M. Huang, F. Zhao, Y. Cheng, N. Xu, and Z. Xu, ACS Nano **3**, 4062 (2009).
[45] A. Borowiec and H. K. Haugen, Appl. Phys. Lett. **82**, 4462 (2003).
[46] L. Chen, X.-F. Jiang, Z. Guo, H. Zhu, T.-S. Kao, Q.-h. Xu, G. W. Ho, and M. Hong, J. Nanomat. **2014**, Article ID 652829 (2014).
[47] G. Vijaya Prakash, M. Cazzanelli, Z. Gaburro, and L. Pavesi, J. Appl. Phys. **91**, 4601 (2002).
[48] S. Vijayalakshmi, M. A. George, and H. Grebel, Appl. Phys. Lett. **70**, 708 (1997).
[49] S. Vijayalakshmi, F. Shen, and H. Grebel, Appl. Phys. Lett. **71**, 3332 (1997).
[50] S. Vijayalakshmi, H. Grebel, Z. Iqbal, and C. W. White, J. Appl. Phys. **84**, 6502 (1998).
[51] G. Schmid, *Clusters and Colloids: From Theory to Application* (VCH, Weinheim, 1994).
[52] P. V. Kamat and D. Meisel, in *Semiconductor Nanoclusters - Physical, Chemical, and Catalytic Aspects*, edited by P. V. Kamat and D. Meisel, Studies in Surface Science and Catalysis Vol. 103 (Elsevier, Amsterdam, 1997).
[53] A. S Edelstein and R. C. Cammarata, *Nanoparticles: Synthesis, Properties and Applications* (Institute of Physics Publishing, Bristol, 1996).
[54] B. A. Smith, D. M. Waters, A. E. Faulhaber, M. A. Kreger, T. W. Roberti, and J. Z. Zhang, J. Sol-Gel Sci. Technol. **9**, 125 (1997).

[55] A. E. Faulhaber, B. A Smith, J. K. Andersen, and J. Z. Zhang, Mol. Cryst. Liq. Cryst. **25**, 283 (1996).
[56] B. A. Smith, J. Z. Zhang, U. Giebel, and G. Schmid, Chem. Phys. Lett. **139**, 270 (1997).
[57] R. H. M. Groeneveld, R. Sprik, and A. Lagendijk, Phys. Rev. B **51**, 11433 (1995).
[58] G. L. Esley, Phys. Rev. Lett. **51**, 2140 (1983).
[59] R. W. Schoenlein, W. Z. Lin, J. G. Fujimoto, and G. L. Eesley, Phys. Rev. Lett. **58**, 1680 (1987).
[60] S. D. Brorson, J. G. Fujimoto, and E. P. Ippen, Phys. Rev. Lett. **59**, 1962 (1987).
[61] C.-K. Sun, F. Vallee, L. H. Acioli, E. P. Ippen, and J. G. Fujimoto, Phys. Rev. B **50**, 15337 (1994).
[62] H. E. Elsayed-Ali, T. Juhasz, G. O. Smith, and W. E Bron, Phys. Rev. B **43**, 4488 (1991).
[63] T. Juhasz, H. E. Elsayed-Ali, G.O. Smith, C. Suarez, and W. E. Bron, Phys. Rev. B **48**, 15488 (1993).
[64] W. S. Fann, R Storz, H. W. K Tom, and J. Boker, Phys. Rev. B **46**, 13592 (1992).
[65] T. S. Ahmadi, S. L. Logunov, and M. A. El-Sayed, J. Phys. Chem. **100**, 8053 (1996).
[66] T. S. Ahmadi, S. L. Logunov, M.A. El-Sayed, J.T. Khoury, and R.L. Whetten, J. Phys. Chem. B **101**, 3713 (1997).
[67] T.W. Roberti, B.A. Smith, and J.Z. Zhang, J. Chem. Phys. **102**, 3860 (1995).
[68] J. K. Hodak, I. Martini, and G. V. Hartland, J. Phys. Chem. B **102**, 6958 (1998).
[69] T. Tokizaki, A. Nakamura, S. Kaneko, K. Uchida, S. Omi, H. Tanji, and Y. Asahara, Appl. Phys. Lett. **65**, 941 (1994).
[70] J. Z. Zhang, Acc. Chem. Res. **30**, 423 (1997).
[71] N. J. Cherepy, D. B. Liston, J. A. Lovejoy, H. Deng, and J. Z. Zhang, J. Phys. Chem. B **102**, 770 (1998).
[72] B. Bescos, R. Hoch, H.-J. Schmidtke, and G. Gerbe, Appl. Phys. B **71**, 373 (2000).
[73] P.T. Anusha, D. Swain, T.S. Prashant, L. Giribabu, S.P. Tewari, and S. Venugopal Rao, J. Phys. Chem. C. **116**, 17828 (2012).
[74] D. Swain, P.T. Anusha, T. Shuvan Prashant, S. P. Tewari, T. Sarma, P. K. Panda, and S. Venugopal Rao, Appl. Phys. Lett. **100**, 141109 (2012).
[75] D. Swain, R. Singh, V. K. Singh, N. V. Krishna, L. Giribabu, and S. Venugopal Rao, J. Mater. Chem. C. **2**, 1711 (2014).
[76] S. Yang, W. Li, B. Cao, H. Zeng, and W. Cai, J. Phys. Chem. C **115**, 21056-21062 (2011).
[77] R. Intartaglia, K. Bagga, A. Genovese, A. Athanassiou, R. Cingolani, A. Diaspro, and F. Brandi, Phys. Chem. Chem. Phys. **14**, 15406 (2012).
[78] K. Abderrafi, R. Garcia-Calzada, M. B. Gongalsky, I. Suarez, R. Abarques, V. S. Chirvony, V. Y. Timoshenko, R. Ibanez, and J.P. Martinez-Pastor, J. Phys. Chem. C **115**, 5147–5151 (2011).
[79] K. Abderrafi, R. Garcia-Calzada, J. F. Sanchez-Royo, V. S. Chirvony, S. Agouram, R. Abargues, R. Ibanez, and J.P. Martinez-Pastor, J. Phys. D. Appl. Phys. **46**, 135301 (2013).
[80] S. Hamad, S. P. Tewari, L. Giribabu, and S. Venugopal Rao, J. Porphy. Phth. **16**, 140 (2012).
[81] S. Minissale, S. Yerci, and L. D. Negro, Appl. Phys. Lett. **100**, 021109 (2012).
[82] S. Dhara, K. Imakita, P. K. Giri, and M. Fujii, Opt. Lett. **39**, 3833 (2014).
[83] B. Bescos, R. Hoch, H.-J. Schmidtke, and G. Gerbe, Appl. Phys. B **71**, 373 (2000).
[84] L. Wang, Q. Li3, H.-Y. Wang, J.-C. Huang, R. Zhang, Q.-D. Chen, H.-L. Xu, W. Han, Z.-Z. Shao, and H.-B. Sun, Light Sci. Applns. **4**, e245 (2015) doi:10.1038/lsa.2015.18.
[85] J. Fuzell, A. Thibert, T. M. Atkins, M. Dasog, E. Busby, J. G. C. Veinot, S. M. Kauzlarich, and D. S. Larsen, J. Phys. Chem. Lett. **4**, 3806–3812 (2013).
[86] K. Bagga, A. Barchanski, R. Intartaglia, S. Dante, R. Marotta, A. Diaspro, C.L. Sajti, and F. Brandi, Laser Phys. Lett. **10**(6), art. no. 065603 (2013).
[87] R. Intartaglia, A. Barchanski, K. Bagga, A. Genovese, G. Das, P. Wagener, E. De Fabrizio, F. Brandi, and S. Barcikowski, Nanoscale **4**(4), 1271 (2012).
[88] M. Yu. Kirillin, E. A. Sergeeva, P. D. Agrba, A. D. Krainov, A. A. Ezhov, D. V. Shuleiko, P. K. Kashkarov, and S. V. Zabotnov, Laser Phys. **25**, 075604 (2015).
[89] X. Li, G. Zhang, L. Jiang, X. Shi, K. Zhang, W. Rong, J. Duan, and Y. Lu, Opt. Express **23**, 4226-4232 (2015).
[90] O. V. Chefonov, A. V. Ovchinnikov, I. V. Ilina, and D. S. Sitnikov, High Temp., In Press, 2015. **DOI:** 10.1134/S0018151X15050077.